Scattering of He atoms from surface defects by grazing-angle diffraction beams

D. Farías,[2] M. Patting,[1] K.-H. Rieder,[1] and J. R. Manson[3]
[1]*Fachbereich Physik, Freie Universität Berlin, Arnimallee 14, D-14195 Berlin, Germany*
[2]*Departamento de Física de la Materia Condensada, C-III Universidad Autónoma de Madrid, Cantoblanco, 28049 Madrid, Spain*
[3]*Department of Physics and Astronomy, Clemson University, Clemson, South Carolina 29634*
(Received 17 July 2001; revised manuscript received 4 January 2002; published 15 April 2002)

It is experimentally demonstrated that diffraction beams from the scattering of He atoms from surfaces can be observed at grazing final angles of up to $\theta_f \approx 90°$ with respect to the surface normal. For He atom scattering from Rh(311) under conditions in which a diffraction beam exits at a grazing angle, a broad scattered intensity appears that is interpreted as diffuse scattering from collisions with the small density of step defects resulting from the unavoidable miscut of the surface. Theoretical models for real and evanescent diffraction beams support the conclusion that this diffuse intensity is due to scattering by step defects from a diffraction beam under grazing exit conditions. For scattering in the plane perpendicular to the direction of the steps, this diffuse scattering signal is much stronger in one direction than in the opposite direction where the crystal azimuthal angle is rotated by 180°. The asymmetry in intensity is interpreted as due to the much larger number of steps up in one direction on the surface due to the crystal miscut, thus such measurements can uniquely determine the miscut direction. This experiment opens new possibilities for the characterization of surface defects with diffraction techniques.

DOI: 10.1103/PhysRevB.65.165435 PACS number(s): 68.35.Dv, 34.50.Dy, 79.20.Rf

I. INTRODUCTION

The study of defects and imperfections is an important part of surface science because, regardless of the degree of cleanliness or the care in preparation, all surfaces include a variety of intrinsic defects that play a large role in the way in which a surface interacts with its environment. He atom scattering has proven to be a very useful tool in the study of surface defects because it is sensitive only to the outermost surface layer and because of the very large total cross sections for scattering from defects. The total cross sections for scattering from isolated adsorbates on a surface is larger than the already rather large cross sections observed for He scattering from similar atomic species in the gas phase.[1] He scattering from intrinsic defects such as vacancies, adatoms or steps is also large.[2] The differential cross sections of surface adsorbates and defects can also be measured through examination of the elastic and inelastic background intensities that appear between the diffraction peaks,[3–5] just as in the case of scattering by other projectiles such as low-energy electron diffraction.[6]

It has been suggested that the extreme sensitivity of He atom scattering to defects is the reason for the lack of success in earlier attempts to carry out experiments with either grazing angle incidence or with diffraction beams at grazing exit angles.[7–9] Under grazing conditions, because the He atom beam travels a long distance close to the surface, the effective number of defects and impurities that the beam encounters becomes large, thus destroying the coherent reflection intensity. However, grazing angle scattering from periodic surfaces is of serious interest because there are a number of interesting effects that should occur whenever a diffraction beam is at grazing exit conditions, where it makes the transition from an evanescent wave to a real diffracted beam. These effects include the threshold resonance,[10–13] skipping phenomena,[14] and the onset of classical chaos.[15]

In this paper we discuss recently reported high-precision diffraction measurements on a well-characterized surface that demonstrate the possibility of observing diffraction of He atom beams under grazing exit conditions.[16] In the neighborhood of grazing exit conditions, where the final diffraction angle $\theta_f \rightarrow 90°$, a broad scattered intensity arises, which is interpreted as incoherent scattering from the He atom diffraction beam by step defects on the surface. These steps are the consequence of the small miscut of the surface, which is unavoidable in the preparation process. Such a miscut implies a larger number of steps up in one direction as opposed to the opposite direction. When the incident beam is oriented perpendicularly to these steps, this diffuse, incoherent signal is much larger for one azimuthal direction than it is for the opposite incident direction where the crystal is rotated by 180°. This asymmetry is interpreted as indicating the direction in which the largest number of steps up occur, thus this measurement can determine the absolute direction of the crystal miscut.

The crystal sample was a well-ordered vicinal surface of Rh(311) with a miscut of less than 0.3°, which implies that the average (311) terrace length between step defects is 200–300 Å. The scattering geometry was such that the incident beam and detector were located in the plane perpendicular to the quasi-one-dimensional corrugations of the fcc(311) surface. For several incident beam energies and for several different diffraction orders, it was found that the diffraction beam intensity near grazing exit decreased approximately linearly as a function of $90° - \theta_f$. Very close to grazing exit conditions, a broad peak in the background intensity was observed, and this peak was considerably larger when the diffraction beam was exiting in the direction that would cause it to collide with the riser faces of the step defects caused by the miscut (i.e., the ''upstairs'' direction as illustrated at the top of Fig. 4). A similar peak, but of much smaller intensity, was observed when the crystal was rotated

 ©2002 The American Physical Society

by 180° and the diffraction beam exited in the ''downstairs'' direction in which it encounters far fewer step risers.

Support for this interpretation is provided by a theoretical model of the scattering from a step edge by a real grazing angle diffraction beam. In the Fraunhofer limit the scattering from a step, when the interference with the back-reflected beam from the large terraces is taken into account, produces an intensity that agrees well with the shape, width, and intensity of the observed intensity.

Recently, a new method has been reported for observing intrinsic surface defects via scattering of the well-defined two-dimensional atomic diffraction beam under bound state resonance (selective adsorption) conditions.[17] This then raises the question of whether the signal observed here might be produced by scattering from the evanescent portion of the grazing angle diffraction beam wave packet. A Fraunhofer-limit theory of scattering of defects by evanescent diffraction beams indicates that, although such scattering does occur, the decay behavior caused by small changes in incident beam angle is much too strong to explain the scattered intensities observed here.

This paper is organized as follows: the next section (Sec. II) describes the experimental apparatus and the protocol of the experiment. Section III discusses the behavior of the observed scattering intensity, Sec. IV develops the theory used to explain the measurements, Sec. V is a discussion of the comparison between theory and experiment, and some conclusions are drawn in Sec. VI.

II. EXPERIMENTAL DESCRIPTION

The He-diffraction experiments reported here were performed with the apparatus described in detail in Ref. 18. The beam was generated by a supersonic nozzle with He-pressures of 70 bars. The energy of the incident He beam can be varied by heating or cooling the nozzle between 800 and 110 K corresponding to wavelengths of 0.34–0.91 Å. The base pressure in the scattering chamber was 8×10^{-11} mbar. The scattered He atoms were detected using a quadrupole mass spectrometer that is mounted on a two-axis goniometer that permits recording a whole set of diffraction spectra at a fixed scattering geometry. Both polar and azimuthal angles of the sample can be freely varied, and the sample can be moved parallel and perpendicular to the surface normal. The polar and azimuthal orientation of the sample was determined to better than 0.2° through measurement of the diffraction peak positions on both the clean and the $c(1\times1)$H phase that, due to its larger corrugation, exhibits many more diffraction peaks.[19,20] This procedure was applied every time the sample was rotated 180° in the azimuthal direction to go from the ''upstairs'' to the ''downstairs'' scattering geometry and vice versa. All spectra shown here have been recorded in the sagittal plane (i.e., in the plane defined by the incident beam and the normal to the surface) with the incoming beam impinging perpendicular to the close-packed rows of the Rh(311) surface. All measurements were performed at a sample temperature of 100 K. The integrated intensities of diffraction peaks shown in Figs. 2 and 3 were obtained after background subtraction of diffraction spectra recorded at different angles of incidence. In order to keep the surface clean during the whole measuring process, the sample was flash annealed to 500 K every 30 min. (to record one spectrum takes approximately 7 min).

The Rh(311) surface was prepared from a large single crystal that was aligned to $\pm0.3°$ with x-ray diffraction, cut with a wire saw, mechanically polished, and electropolished. The surface was first prepared in UHV by repeated cycles of sputtering with 1 keV Ne ions and annealing to 1100 K. Temperatures were restricted to below 1100 K to avoid an irreversible transition to a (1×2)-disordered reconstruction of the substrate.[21] The daily surface preparation consisted of 30-min sputtering, followed by heating 5 min in 1×10^{-8} mbar oxygen at 1000 K and 10 min in 1×10^{-8} mbar hydrogen at 500 K. The cleanliness of the sample was judged by the sharpness of the diffraction peaks in the He spectra of the clean surface and by the ability to reproduce the low-coverage hydrogen phases at $T=100$ K, as these are very sensitive to the presence of impurities on the surface.

III. EXPERIMENTAL OBSERVATIONS

Two typical intensity spectra are exhibited in Fig. 1 for the case of a He beam incident on the Rh(311) surface with a polar angle of $\theta_i=50°$ and in the azimuth perpendicular to the close-packed rows on this vicinal surface. The incident energy is $E_i=65.7$ meV corresponding to a de Broglie wavelength of $\lambda=0.56$ Å and a wave vector $k_i=2\pi/\lambda=11.2$ Å^{-1}. The incident angle is somewhat smaller than the critical angle $\theta_c=60.8°$ for which the (01) diffraction peak becomes evanescent. One of the two spectra, shown as a solid curve, is taken in the ''upstairs'' direction, and the other shown as a dashed curve, is in the ''downstairs'' direction. Figure 1 clearly demonstrates the similarity of the diffraction patterns taken in the two opposite directions. The large diffraction peaks visible are the (00) specular, as well as the (0,1), $(0,\overline{1})$, and $(0,\overline{2})$ peaks, and in addition there are small $(0,\overline{3})$ and $(0,\overline{4})$ peaks. The region of interest in this work is the range $70°<\theta_f<90°$ into which the (01) beam scatters intensity as it interacts at grazing exit with the widely spaced steps due to the miscut of the crystal.

Figures 2 and 3 show the integrated diffraction peak intensities as a function of incident polar angle θ_i for two different energies. Figure 2 is for $\lambda=0.56$ Å as in Fig. 1, while Fig. 3 is for $\lambda=0.80$ Å that corresponds to the energy $E_i=33$ meV, wave vector $k_i=7.9$ Å^{-1}, and a critical angle for emergence of the (01) diffraction $\theta_c=55.1°$. The data in both of these figures were taken in the upstairs direction, but nearly identical intensities are obtained in the downstairs direction. Including the specular, at the higher energy a total of seven diffraction peaks are observed over the measured range of incident angles $35°<\theta_f<90°$, while at the lower energy five diffraction beams are seen. An important point is the nearly linear decrease of the (01) diffraction peak in the variable $90°-\theta_f$ as $\theta_i\rightarrow\theta_c$. This linear dependence is also visible in Fig. 2 for the high-energy (02) diffraction peak as it approaches evanescent behavior at $\theta_i=48°$. Another inter-

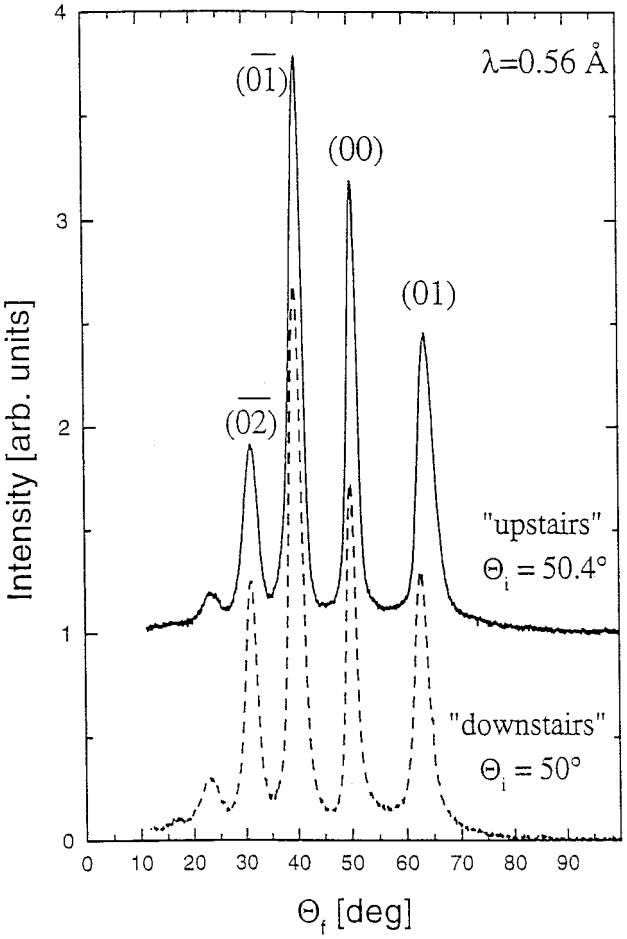

FIG. 1. Two typical measured He atom scattering intensity spectra from Rh(311) for $E_i = 65.7$ meV ($\lambda = 0.56$ Å, $k_i = 11.2$ Å^{-1}) and an incident angle $\theta_i = 50°$. The curve shown as a solid line is taken in the ''upstairs'' direction, while the dashed curve is for the ''downstairs'' direction.

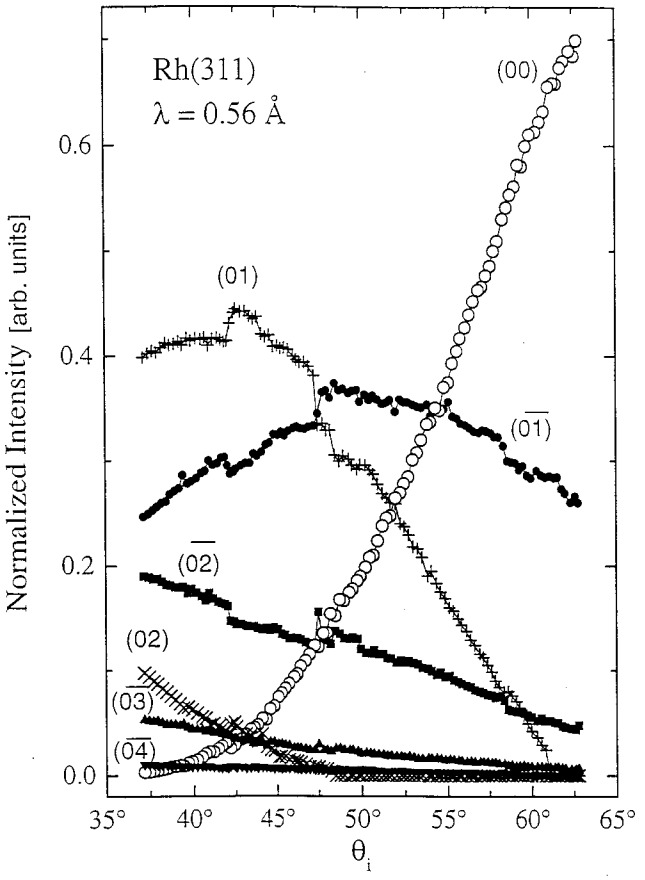

FIG. 2. Integrated intensities of the diffraction peaks as a function of incident polar angle for a He atom beam of wavelength $\lambda = 0.56$ Å ($E_i = 65.7$ meV) impinging on a Rh(311) surface.

esting point is that there is no evidence for a threshold resonance[10–13] in the neighborhood of θ_c, which would be manifest by a sharp decrease in intensity of the emerging diffraction peak and a corresponding sharp resonance behavior in the other diffraction peaks. This is consistent with previous calculations which predict that the threshold effects will be negligible for He scattering from the relatively soft, weakly corrugated potentials of metal surfaces.[13]

Figure 4 shows in more detail the observed scattered intensity as a function of θ_f in the vicinity of 90° for several incident angles near $\theta_i = \theta_c$ for the (01) diffraction order. Both of the two incident energies of Figs. 2 and 3 are shown. For each incident energy the panel on the left is for the (01) diffraction beam pointing in the ''upstairs'' direction (as illustrated at the very top of Fig. 4) and the panel on the right is for the ''downstairs'' configuration. There is a broad peak that remains nearly stationary at very nearly the same value of θ_f that becomes less intense as θ_i approaches θ_c, and disappears completely for θ_i a little larger than θ_c. What is striking, however, is that this peak is much larger in the ''upstairs'' direction than for the ''downstairs'' direction. For similar values of θ_i close to θ_c the intensity in the ''upstairs'' direction is approximately an order of magnitude larger. The intensity of the peak decreased rapidly with increasing azimuthal angle away from the plane perpendicular to the steps, and disappeared when the crystal azimuth was rotated by as much as 10°.

This anomalously large scattering signal in the ''upstairs'' direction is interpreted as scattering of the He atoms out of the (01) diffraction beam caused by collisions with the faces of the step defects produced by the slight miscut of the surface. Because of the miscut, a systematic error is induced in the surface, which causes many more step riser faces to appear in the upstairs direction than in the ''downstairs'' direction, hence the large differences in observed intensity in the two opposing crystal azimuths.

This large discrepancy in the two crystal azimuthal orientations (i.e., with the steps oriented either 90° or 270° with respect to the scattering plane) cannot be due to a large asymmetry in the periodic corrugation of the Rh(311) terraces, since it is well known that symmetric corrugation functions are adequate to describe He diffraction even for seemingly asymmetric stepped surfaces such as the Ni(115) and Cu(112).[22] On Rh(311), this is verified both by our direct measurements, which show negligible differences in diffraction beam intensity spectra for the two crystal orientations, as seen in Fig. 1. It is also supported by the fact that the total diffraction intensities in Figs. 2 and 3 are independent of the

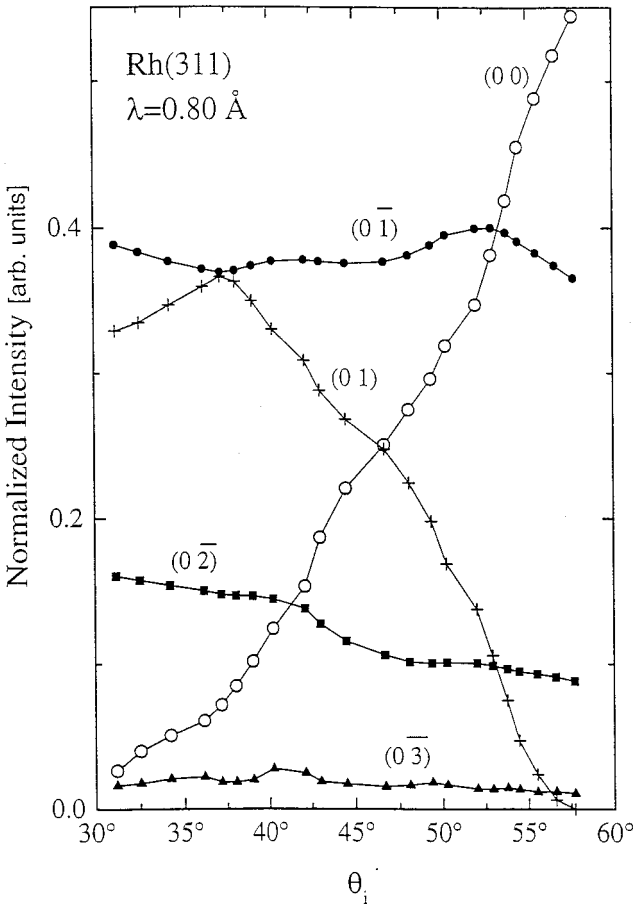

FIG. 3. Same as Fig. 2 except for an incident beam of wavelength $\lambda = 0.80$ Å ($E_i = 32$ meV).

two azimuths, and by elastic close coupling calculations using the known potential for this surface,[19] which predict that the differences in diffraction intensities in the two orientations are less than 10%. Another possible alternative explanation is that the anomalous intensity seen in Fig. 2 is due to scattering from the same defects by the evanescent tail of the (01) diffraction beam. However, this possibility can be ruled out because simple calculations, discussed in Sec. IV B below, show that the short-range exponential decay of an evanescent beam away from the surface would cause its defect-scattering intensity to decrease much faster for $\theta_i > \theta_c$ than is observed in Fig. 4.

Figure 5 shows the same data as in Fig. 4, as well as additional data for the same two incident energies, but here the data is shown with a linear background subtracted off. Also plotted in Fig. 5 are theoretical curves for the intensity scattered from the steps due to the crystal miscut, as discussed below in Secs. IV and V. Theoretical curves are shown only for incident angles close to and greater than the critical angle, because at smaller incidence angles the signal becomes dominated by the diffraction beam intensity that is not included in the calculated curves. This figure shows even more clearly the large asymmetry between scattering in the downstairs and upstairs directions as can be seen upon comparing intensities at similar angles. For example, for $\lambda = 0.79$ Å, at $\theta_i = 55.4°$, very close to the critical angle of $\theta_c = 55.3°$, the maximum measured intensity in the upstairs direction is about 38 (in our relative units), while in the downstairs direction the corresponding intensity is only about 5. Similarly, for $\lambda = 0.56$ Å, the measurements closest to the critical angle $\theta_c = 60.8°$ give an intensity of 20 in the upstairs direction, while in the downstairs direction it is only about 3. In both cases this is an order-of-magnitude difference. On the other hand, at incidence angles of 1°–2° smaller than the critical angles, where the intensity is mainly directly from the diffraction peak, the intensities in the upstairs and downstairs directions are comparable.

A further example of scattering spectra near the critical angle is shown in Fig. 6 for the slightly longer de Broglie wavelength $\lambda = 0.85$ Å ($E_i = 28$ meV, $k_i = 7.4$ Å^{-1}). As in Figs. 4 and 5, the upper panel shows the measured data, while the lower panel shows the same data with a linear background subtracted. Only scattering in the upstairs direction is shown. Again, very close to the critical angle $\theta_c = 54°$, the broad scattering signals from the steps due to the miscut are visible.

IV. THEORY

The conditions for grazing exit are the same as those for a real diffraction beam to become an evanescent beam, thus the scattering may be due to either scattering from the grazing diffraction beam or from the barely evanescent beam. The scattering of both real and evanescent diffraction beams will be considered here, and we show that the observed signals of Fig. 5 are due to the real diffraction. Scattering from an evanescent diffraction beam is shown to decay too rapidly when the incidence angle is larger than the critical angle, and will not be observable in this experiment.

A. Step scattering by a grazing angle diffraction beam

The surface is approximated by a rigid corrugated wall and the effects of an attractive adsorption well in the potential are ignored. The basic features of the scattering process are readily described by semiclassical quantum scattering theory in the Fraunhofer limit. The grazing exit diffraction beam near the critical angle can be viewed as a plane wave traveling parallel to the surface with a wave vector of magnitude $|\mathbf{K}_i + \mathbf{G}| \approx k_i$, where $\mathbf{K}_i$ is the component of the incident wave vector $\mathbf{k}_i$ parallel to the surface ($K_i = k_i \sin\theta_i$) and $\mathbf{G}$ is the surface reciprocal lattice vector. In this configuration of in-plane scattering perpendicular to the one-dimensional surface corrugation, $G = 2\pi/d$, where $d = 4.455$ Å is the corrugation period. Only steps up will be considered, since a step down is shadowed by the terrace above and it will not scatter appreciably. An isolated step-up defect then, in the simplest terms, becomes an opaque linear obstacle of width a in the path of the diffraction beam. According to Babinet's principle, the scattering amplitude from an opaque obstacle can be replaced by a similarly shaped slit in an opaque sheet. The angle that the step riser face makes with the surface plane is not important at this level of approximation, and the scattering amplitude is the standard Fraunhofer expression

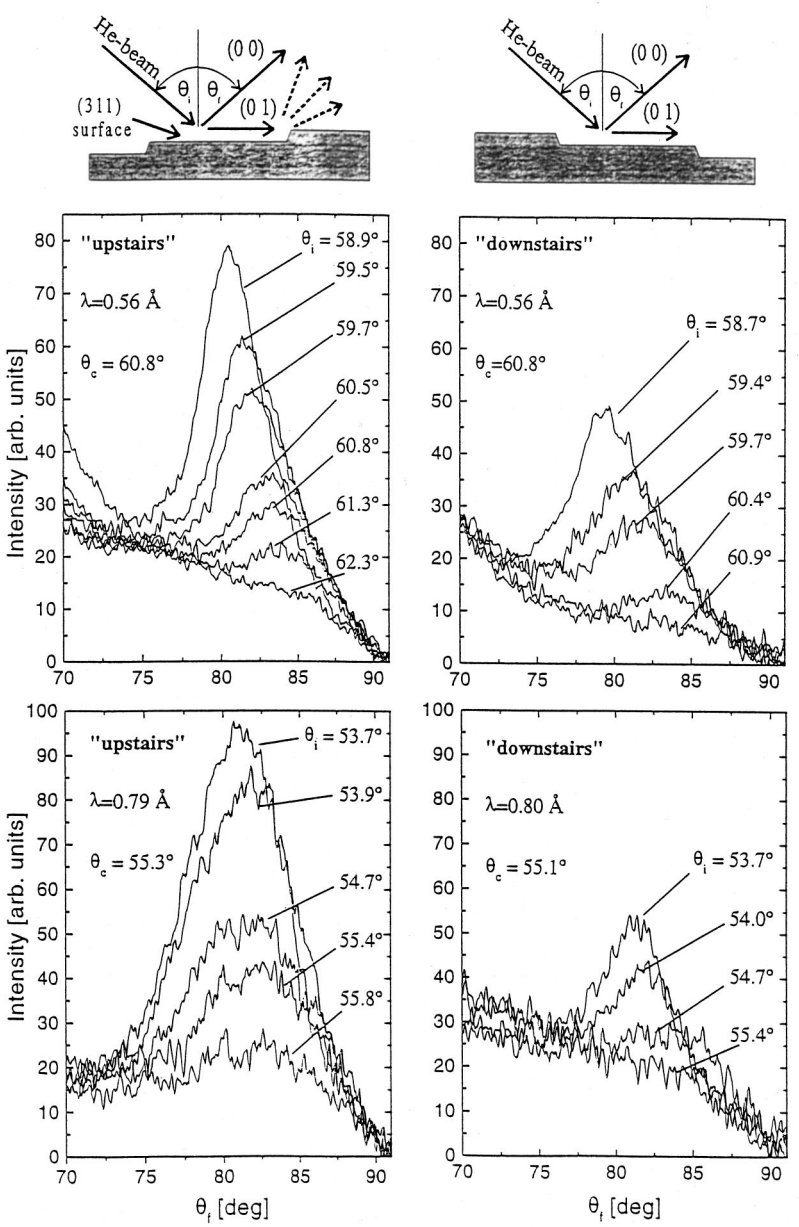

FIG. 4. Measured scattered intensity as a function of final angle θ_f for several incident angles θ_i very close to the critical angle for the disappearance of the (01) diffraction peak. The upper two panels are for an incident wavelength $\lambda = 0.56$ Å where the critical angle is $\theta_c = 60.9°$ and the lower panels are for $\lambda = 0.8$ Å or 0.79 Å as marked, where $\theta_c = 55.1°$ or 55.3°. The panels on the left are for the (01) diffraction beam pointing in the ''upstairs'' direction and those on the right show the ''downstairs'' direction. The insert at the top illustrates the upstairs and downstairs scattering configurations.

$$A(\kappa) = \frac{2A_0}{\kappa} e^{-i\kappa a/2} \sin(\kappa a/2), \tag{1}$$

where A_0 is the amplitude of the diffraction beam and $\kappa = k_i \cos\theta_f$.

However, when the diffraction beam strikes the step defect it is scattered both toward and away from the surface. That part of the scattered amplitude which is scattered towards the surface will be reflected back by the smooth terrace at the top of the step, and this back-reflected amplitude will interfere with the directly scattered part to give rise to an observable signal. Including the back reflection from the mirror surface implies that the total scattering amplitude is given by

$$A_T(\kappa) = A(\kappa) - e^{2i\kappa b} A(-\kappa), \tag{2}$$

where the parameter b in the phase factor is the height chosen for the plane of reflection relative to the terrace plane at a distance $z = a$ above the surface. Apart from a trivial phase factor this leads to

$$A_T^D(\kappa) = \frac{4A_0}{\kappa} \sin(\kappa a/2) \sin(\kappa[b + a/2]). \tag{3}$$

The simplest and most logical choice for the position of the reflecting plane is to make it coincident with the top of the terrace that corresponds to $b = 0$ leading to the following expression for the scattered intensity:

$$I(\theta_f) \propto \frac{I_G}{\kappa^2} \sin^4\left(\frac{\kappa a}{2}\right), \tag{4}$$

where I_G is the intensity of the grazing diffraction beam given by

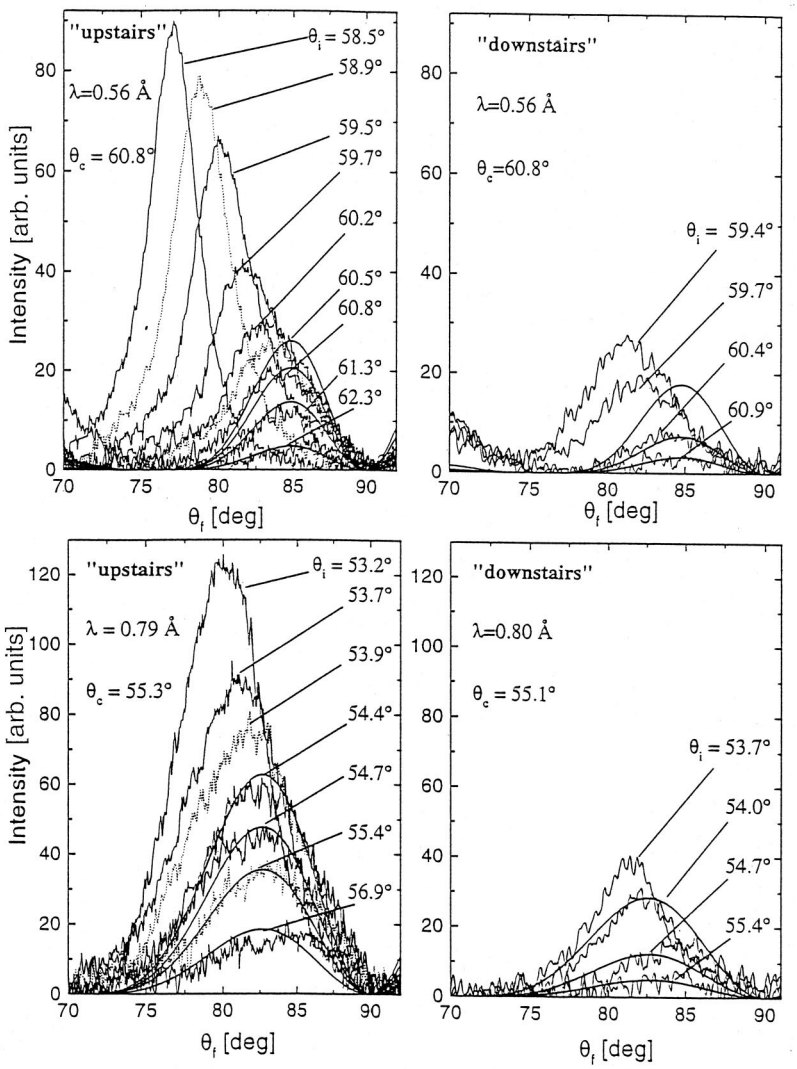

FIG. 5. The same data as shown in the "upstairs" and "downstairs" panels of Fig. 4, after background subtraction, are compared with theoretical predictions (smooth solid curves) of the scattered intensity due to scattering from widely spaced step face defects. Calculated curves are shown only for angles close to or greater than the critical angle.

$$I_G(\theta_i,\theta_f)=\frac{\cos\theta_f}{\cos\theta_i}|A_G|^2. \tag{5}$$

The diffraction beam amplitude A_G also has a dependence on θ_i and θ_f, and it can be directly calculated for a periodic surface, for example, using the coupled channels formalism.[19] The behavior of $|A_G|^2$ is expected to be smoothly varying as θ_i crosses the critical angle θ_c, unless there happens to be a bound state of the potential very close to the top of the adsorption well, in which case $|A_G|^2$ will exhibit resonance behavior for θ_i on the evanescent side of θ_c. This resonant behavior is often manifest as a sharp maximum, but may also be a minimum.[23,24] For the surface measured in this work, elastic coupled channels calculations[19] using the well-established He-Rh(311) potential[19] show that the amplitude $A_{(01)}$ for the (01) beam is nearly constant in the region of the critical angle, as seen in Fig. 7.

Figure 7 shows calculations for $\lambda=0.56$ Å of the square modulus of the (01) diffraction peak amplitude $|A_{(01)}|^2$ as well as the intensity $I_{(01)}$ of the (01) peak as given by Eq. (5). Although the intensity of the (01) diffraction peak decreases strongly near $\theta_i=\theta_c$ and vanishes at θ_c, the squared diffraction amplitude is a smoothly varying function and exhibits no unusual behavior. The very sharp peak in $|A_{(01)}|^2$ seen at $\theta_i=60.99°$ is due to the selective adsorption resonance of the evanescent (01) diffraction beam with the highest ($n=3$) bound state of the interaction potential located at an energy of $\epsilon_3=-0.48$ meV. Thus, the above arguments show that the linear dependence of $I_{(01)}(\theta_i)$ as exhibited in Figs. 2 and 3 is explained by the θ_f dependence of the flux factor $\cos\theta_f/\cos\theta_i$ in Eq. (5).

B. Step scattering by an evanescent beam

Next we consider the scattering of an evanescent diffraction beam by the same surface step riser as in Sec. IV A. As opposed to a grazing-angle diffraction beam, the asymptotic form of the wave function of an evanescent beam is exponentially damped away from the surface,

$$\Psi_{\mathbf{G}}(\mathbf{r})=e^{i(\mathbf{K}_i+\mathbf{G})\cdot\mathbf{R}}e^{-k_{\mathbf{G}z}z}, \tag{6}$$

where z is the direction normal to the surface and the position vector is divided into components parallel and normal to

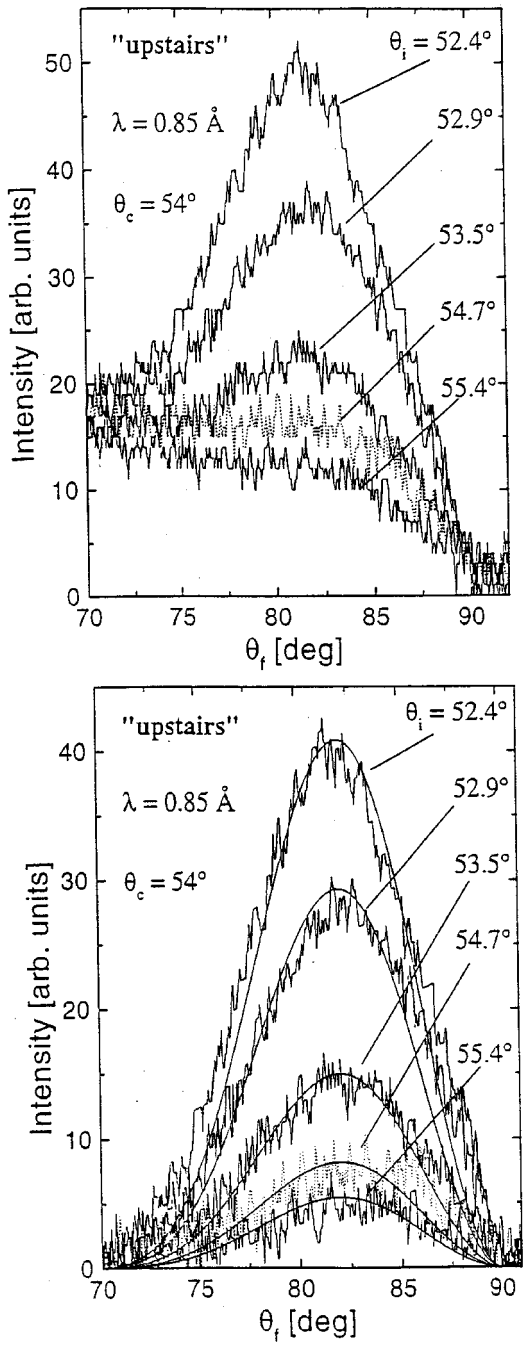

FIG. 6. A series of intensity spectra similar to those of Figs. 4 and 5, taken in the upstairs direction, for a de Broglie wavelength of $\lambda = 0.85$ Å^{-1}. The upper panel shows the data as measured, and the lower panel is the same data with a linear background subtracted and the solid curve is the theoretical calculation.

the surface according to $\mathbf{r}=(\mathbf{R},z)$. The conservation of energy and parallel momentum determine the evanescent perpendicular wave vector as

$$k_{\mathbf{G}z}=|\sqrt{k_i^2-(\mathbf{K}_i+\mathbf{G})^2}|. \tag{7}$$

Adopting the Rayleigh ansatz,[25] the asymptotic form of Eq. (6) can be extended right up to the surface.

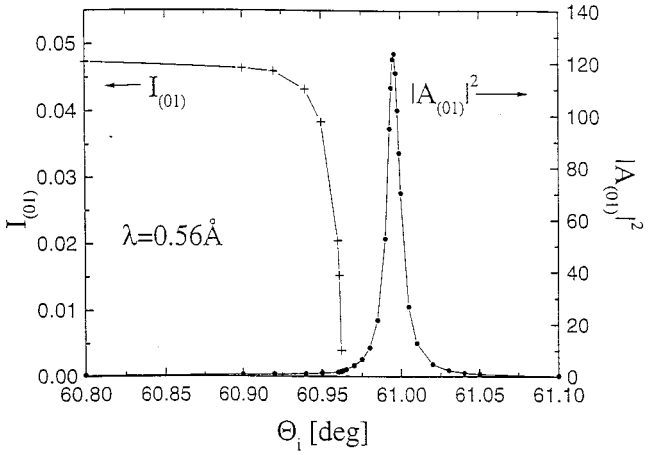

FIG. 7. The calculated square modulus $|A_{(01)}|^2$ of the (01) diffraction beam, and the diffraction intensity $I_{(01)}(\theta_i)$ for He scattering from Rh(311) for the incident angle θ_i in the vicinity of the critical angle θ_c. $\lambda = 0.56$ Å and $\theta_c = 60.96°$

Again, as in Sec. IV A above, the step is regarded as a one-dimensional barrier extending upwards from the surface a distance a in the z direction and the azimuth of the incident beam is taken to be perpendicular to the steps. The scattering amplitude in the Fraunhofer limit can be calculated using the standard form for the transmission amplitude of a wave incident on a diffraction grating,[26] given by

$$A(\kappa)=A_0\int_{-\infty}^{+\infty}t(z)e^{-i\kappa z}dz, \tag{8}$$

where as before $\kappa=(K_i+G)\cos\theta_f\approx k_i\cos\theta_f$ and $t(z)$ is the transmission function. For the present case of illumination of the step by an evanescent beam, the transmission function becomes

$$t(z)=\begin{cases}0; & z<0\\ 0; & 0<z<a\\ A_0e^{-k_{\mathbf{G}z}z}; & z>a.\end{cases} \tag{9}$$

As in Eq. (2) above, the observed amplitude must include the back reflection from the mirror surface leading to an expression for the total scattering amplitude given by

$$A_T^E(\kappa)=\frac{-2iA_0}{\kappa^2+k_{\mathbf{G}z}^2}[\kappa\cos\kappa(a+b) + k_{\mathbf{G}z}\sin\kappa(a+b)]e^{i\kappa b-k_{\mathbf{G}z}a}. \tag{10}$$

For scattering by an evanescent wave, the scattering amplitude of Eq. (10) plays the same role as Eq. (3) above for a real grazing angle diffraction beam.

It is interesting to compare the behavior of Eqs. (3) and (10). This is done in Fig. 8 for the case where the position of the mirror surface is taken to be the top of the terrace, $b=0$. The solid line shows the squared amplitude $|A_T^D|^2$ of Eq. (3) as a function of final angle θ_f for the (01) diffraction beam and the $\lambda = 0.79$ Å case shown in Fig. 4. The dashed line shows $|A_T^E e^{+k_{\mathbf{G}z}a}|^2$ for the same case, but where the

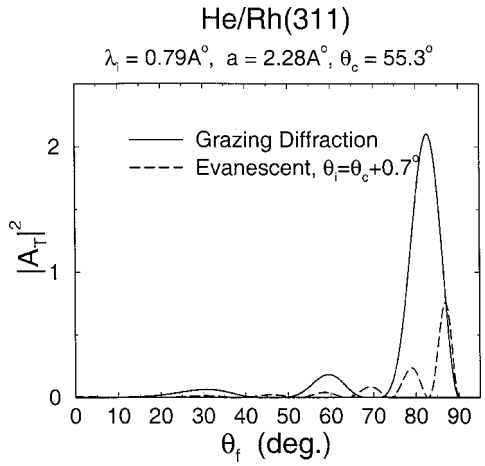

FIG. 8. The square modulus of the scattering amplitude plotted as a function of final angle. The solid curve is $|A_T^D|^2$ of Eq. (3) for scattering by a grazing exit diffraction beam corresponding to the $\lambda = 0.79$ Å case of Fig. 5, and the dashed curve is $|A_T^E e^{+k_{Gz}a}|^2$ of Eq. (10) for scattering by an evanescent wave for the same system with $\theta_i = \theta_c + 0.07°$.

incident angle is $\theta_i = 56°$, slightly larger than the critical angle of $\theta_c = 53.3°$. Both functions show quadratic behavior in $90° - \theta_f$ very close to the forward direction, they have a large first maximum, and smaller maxima as κ increases.

The comparison shown in Fig. 8 is slightly misleading, however, because it does not exhibit the exponential decay of the intensity caused by the factor $e^{-2k_{Gz}a}$. The step height a is expected to be larger than 1 Å, and the evanescent wave vector k_{Gz} increases with increasing θ_i and very quickly becomes comparable to the incident wave vector that is of order 6–10 $Å^{-1}$, so the exponential decay is very strong. For example, in the case of Fig. 8 where θ_i exceeds θ_c by only 0.7°, $k_{Gz}a \approx 2$ and $e^{-2k_{Gz}a} \approx 0.02$. It is this rapid decay of the intensity that excludes scattering from evanescent waves from being the cause of the scattering signals seen in Figs. 4 and 5. Also Fig. 8 shows that the intensity for scattering by the evanescent wave would not agree with data such as that shown in Fig. 5 because it oscillates too rapidly and the tallest peak is too narrow in width.

V. COMPARISON OF THEORY WITH DATA

Comparisons between the experimental measurements and the theory of scattering of the grazing angle diffraction beam from isolated steps is shown in Figs. 5 and 6. However, before discussing the significance of these comparisons, it is necessary to develop a method of normalizing the calculated intensities to those of the experiment, and to take account of the experimental width of the incident beam, which causes an even larger width of the grazing diffraction beam.

The relative intensities of the theoretical curves at each value of θ_i are determined from the observed linear dependence of the (01) diffraction peak intensity for $\theta_i < \theta_c$ and by assuming that the incident beam has a Gaussian distribution in angular spread about its center, both in and out of the scattering plane. The full width at half maximum (FWHM)

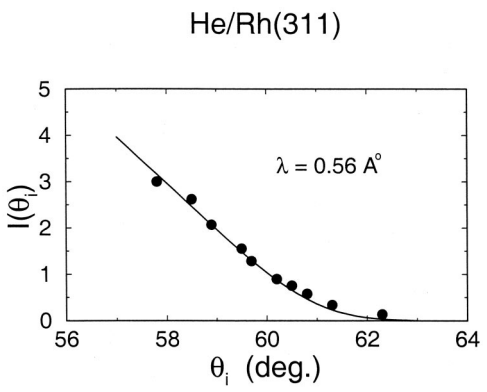

FIG. 9. Maximum peak intensity as a function of θ_i for the $\lambda = 0.56$ Å case of Fig. 5. The solid curve is the intensity calculated from Eq. (11) and the filled circles are the maximum peak intensities from Fig. 5.

of the Gaussian is chosen to be the measured FWHM of the specular beam, which is $\sigma = 1.85°$. The FWHM of the specular beam is substantially larger than that of the incident beam because of the proximity of the detector to the crystal, the source-to-crystal distance being approximately 0.5 m while the detector is only 4.0 cm from the sample. Thus, the intensity $I_{(01)}(\theta_i)$ is chosen according to the formula

$$I_{(01)}(\theta_i) = \frac{S}{\sqrt{\pi}\sigma} |A_{(01)}|^2 \int_{-\infty}^{\theta_c - \theta_i} e^{-\theta^2/\sigma^2} (\theta_c - \theta_i - \theta) d\theta. \tag{11}$$

For θ_i sufficiently smaller than θ_c and assuming $|A_{(01)}|^2$ to be approximately constant, $I_{(01)}(\theta_i)$ appearing in Eq. (4) is a linear function, in agreement with the linear intensity of the grazing angle diffraction beam near θ_c exhibited in Figs. 2 and 3. However, for θ_i very close to, or even slightly larger than θ_c, $I_{(01)}(\theta_i)$ of Eq. (11) accounts for the fact that, although the leading edge of the incident beam distribution is greater than θ_c, the trailing edge still produces a real diffraction intensity. The normalization of calculations to experiment is then effected by choosing the constant S so that the calculated curve matches the experimental curves for one of the spectra at a given θ_i such as shown in Fig. 5. The combination of Eqs. (11) and (4) are the theoretical expressions used to compare with the experimental data, and aside from the overall normalization constant S, this is a single parameter theory depending only on the step height a.

The agreement of Eq. (11) with the measured data is exhibited in Fig. 9. There, for the $\lambda = 0.56$-Å case of Fig. 5 in the upstairs direction, the solid curve is the intensity calculated from Eq. (11) while the solid circles are the maximum peak intensity of the measured spectra, plotted as a function of incident angle θ_i. This figure shows that there is significant intensity observed even for $\theta_i > \theta_c$. For θ_i smaller than θ_c by more than 1°, the data exhibit the expected linear behavior of the real diffraction beam.

The solid curves in Figs. 5 and 6 are the theoretical predictions of Eq. (4) with $I_{(01)}(\theta_i)$ chosen according to Eq. (11). For example, in the upstairs direction, Fig. 5 shows good agreement between the observed scattering distribution

and the theoretical model of Eq. (4) for values of θ_i ranging from slightly less than θ_c to significantly larger than θ_c, where only the trailing portion of the incident beam distribution produces a real (01) diffraction beam. The shape and width of the theoretical curves, the stationary position of the peak maximum, and the decrease in intensity with increasing θ_i are all well predicted for a value of $a=2.28$ Å, which is exactly twice the minimum step height for this surface. Theoretical curves are shown only for incident angles θ_i near or larger than the critical angle θ_c because for smaller incidence angles the scattering gradually becomes dominated by the diffraction peak that is not included in the theory. In the downstairs direction shown in Fig. 5 (where fewer measured spectra are available), equally good agreement between theory and experiment is obtained, but quite remarkably, the overall intensities at equivalent values of θ_i close to or larger than θ_c are approximately an order of magnitude smaller than those for the upstairs direction. Figure 6 also shows similar agreement between theory and experiment in the vicinity of $\theta_i \approx \theta_f$, although in this case the data were taken only in the upstairs direction. The agreement between theory and experimental data, taken together with the large difference in signal intensity between the upstairs and downstairs directions, indicates that the scattered intensity is due to the steps created by the miscut and that furthermore the direction with the most steps-up can be distinguished. However, no independent measurements with any technique other than helium atom scattering were performed to verify the presence of steps or the miscut direction.

The minimum step height on the fcc(311) surface is $a=1.14$ Å. A defect with exactly twice this value could be indicative of double-height steps, or of defects consisting of a ''minifacet'' of two adjacent single steps. The present theoretical model would give the same results for both cases. Concerning single steps, which in addition to double steps have been shown to be present at this surface,[27] our model predicts that they would produce a much broader feature, essentially twice as broad as that of the double steps, centered at about $\sim 75°$ in Fig. 5. As a consequence, this signal could not be distinguished from the background in our experiments.

There are also some interesting peculiarities of a fcc(311) surface that should be discussed in connection with these He scattering measurements. A step up and a step down in the (311) surface are not equivalent, even though both have the same height of 1.14 Å. If the step up riser face is a (100) crystal plane then the step down face will be a (111) plane (or exactly the contrary, if the crystal azimuth is rotated by 180°). Both of these faces consist of close-packed rows, but the tilt angle of the (100) and (111) crystal planes relative to the (311) surface differs by approximately 5°. As indicated above, this small difference in tilt angle has no effect on the theoretical interpretation of the intensity of Eq. (4), and at this level of analysis the intensity projected in the direction for θ_f near 90° will be the same for both types of step faces.

However, the direct semiclassical scattering from the step face will produce an approximately Fraunhofer scattering pattern centered about the direction specular to the step face. In a different context a similar specular-to-the-step-face scattering was recently observed by some of the present authors as a result of scattering directly from the incident beam.[27] In this experiment, scattering patterns were observed as features in the diffuse elastic background between diffraction peaks. These features were analyzed in terms of single slit Fraunhofer intensities for both single and double steps, and were observed at a scattering angle corresponding to the specular angle of the incident beam relative to the step faces of steps on the (311) surface. This work provides confirmation that both single and double steps exist on the Rh(311) surface. In order to attain sufficient intensity, however, it was necessary to enhance the step density on the surface by a sputtering process. The results found in Ref. 27 would then indicate that scattering of a grazing angle diffraction beam from a (111) step face, which makes a tilt angle of 29.50° with respect to the (311) surface plane, would produce a Fraunhofer pattern at approximately $\theta_f \approx 30°$, while the (100) step face plane that makes a tilt angle of 25.24° would produce a similar pattern but at $\theta_f \approx 40°$. (In the previous experiments, the actual angles were found to be slightly less than those predicted by the crystal plane angles, an effect that was attributed to a small change in step face inflection angle due the Smulowchowski smoothing of the electron density.[27]) Such a pattern was looked for in this experiment but not observed. There are two reasons why the step face Fraunhofer pattern could not be seen: (1) the intensity of the (01) diffraction peak is small and the step density is low (e.g., in the case of Ref. 27 in which these patterns were observed from the incident beam, the surface step density was enhanced by sputtering) thus the intensity will be small; and (2) at all incident energies investigated, for $\theta_i \approx \theta_c$ a value of $\theta_f \approx 30°$ or 40° falls very close to the rather large $(0,\overline{3})$ and $(0,\overline{2})$ diffraction peaks and hence the signal could not be distinguished from the background.

One other characteristic of the (311) surface is that after a step up or a step down, the phase of the (311) terraces is shifted by one-half of an atomic spacing. Thus adjacent (311) terraces differing in height by one step are out of phase in the direction parallel to the steps. After a double step, the terraces are back in phase. However, this subtle phase shift should have no measurable effect on the He atom scattering intensities because the corrugations of the (311) surface in the direction parallel to the steps are small. He scattering measurements performed in the direction parallel to the steps on this Rh(311) face, i.e., in the crystal azimuth of 0° or 180°, showed no detectable diffraction peaks in the sagittal plane, indicating a negligible corrugation of the interaction potential.

VI. CONCLUSIONS

This work demonstrates that atomic diffraction by periodic surfaces can be observed all the way to the critical angle where the diffraction beam exits parallel to the surface plane. Under these critical conditions we observe an anomalously large, broad and diffuse scattering intensity that can be attributed to scattering out of the grazing angle diffraction beam caused by step defects as a result of the crystal miscut. This conclusion is supported by comparisons with calcula-

tions of the expected scattering distribution due to such defects, and it is supported by the observation that the intensity is roughly an order of magnitude larger in the ''upstairs'' direction than in the ''downstairs'' direction, with the ''upstairs'' direction corresponding to the crystal orientation that would produce the largest density of step defects with risers facing the exiting diffraction beam. This large discrepancy in the two crystal azimuthal orientations (i.e., with the steps oriented either 90° or 270° with respect to the scattering plane) cannot be due to the slight asymmetry in the periodic corrugation of the Rh(311) terraces. This is verified both by our direct measurements, which show negligible differences in diffraction beam intensities for the two crystal orientations, and by elastic close coupling calculations[19] using the known potential for this surface,[19] which predict that the differences in diffraction intensities in the two orientations are no more than 10%. Thus, one of the major conclusions of this work is that the large asymmetry in signal intensity in the two opposite directions is due to the much larger density of step-up faces in one of the two directions caused by the miscut of the crystal. This allows unambiguous determination of the miscut direction in He atom scattering experiments.

The theoretical model for scattering from step faces predicts that the intensity distribution should have the same shape in both the upstairs and downstairs directions because appreciable scattering occurs only at the steps up (and not at the steps down), and this is clearly verified in the comparisons of Fig. 5. The difference in overall intensity is predicted to be proportional to the step density, thus the order of magnitude difference in intensity indicates a similar difference in numbers of steps up in the two opposite directions.

One possible alternative explanation of the observed results would arise if the crystal orientation in the polar angle were unknown to up to $\Delta\theta_i = 2°$. Then the observed signal could be explained as the direct observation of the tail of the roughly Gaussian-shaped grazing angle diffraction beam as this beam passed from real to evanescent state. However, measurements of the angular positions of the rather large number of other diffraction peaks allows the uncertainty in crystal orientation to be no more than 0.2°. Consequently, such an explanation can be ruled out.

Another possible explanation is that the observed signal could be scattering by the step faces from the evanescent part of the grazing angle diffraction beam. The evanescent parts of the wave packet are strongly localized close to the surface by their exponential amplitude decay in the direction perpendicular to the surface. However, a scattering model similar to that developed for grazing angle diffraction beam scattering shows that the intensity from evanescent waves is strongly damped as a function of incident beam angle and thus cannot be the source of the large signals seen here.

Finally, it is of interest to discuss some future possibilities for application of this effect:

(i) The quantitative study of grazing exit diffraction will enable measuring the differential and total cross sections of surface defects under the well-defined conditions of an illuminating beam traveling parallel to the surface. This is of fundamental interest because it permits observation of scattering from defects illuminated by a two-dimensional wave, rather than the usual conditions of illumination in a full three-dimensional geometry.

(ii) There are some intriguing possibilities for inelastic scattering effects. If the surface is contaminated with adsorbates having low-energy modes, such as frustrated translation modes,[28] there should be inelastic Einstein mode multiquantum overtones scattered out in all directions by these defects. We would expect the grazing exit diffraction beam to impart large parallel momentum transfers and hence produce large inelastic intensities.

(iii) This effect is not limited to atom or molecule scattering, it should be observed in electron scattering, photon scattering, or any other scattering process in which the periodic surface produces diffraction beams that can have significant intensity near grazing exit conditions.[29,30]

ACKNOWLEDGMENTS

The authors would like to thank Dr. Henrik Tröger for carrying out useful calculations and for helpful discussions. One of us (J.R.M.) would like to express appreciation to the Department of Physics of the Freie Universität Berlin for hospitality during part of this work. This work was supported by the U.S. Department of Energy under Grant No. DE-FG02-98ER45704, by the National Science Foundation under Grant No. DMR-0089503, and by the Deutsche Forschungsgemeinschaft under the Sonderforschungsbereich 290 (TP A5).

[1] B. Poelsema and G. Comsa, in *Scattering of Thermal Atoms from Disordered Surfaces*, edited by G. Höhler, Springer Tracts in Modern Physics 115 (Springer Verlag, Heidelberg, 1989).

[2] L. K. Verheij, B. Poelsema, and G. Comsa, Surf. Sci. **162**, 858 (1985).

[3] A. M. Lahee, J. R. Manson, J. P. Toennies, and Ch. Wöll, J. Chem. Phys. **86**, 7194 (1987); W. A. Schlup and K.-H. Rieder, Phys. Rev. Lett. **56**, 73 (1986).

[4] A. M. Lahee, J. R. Manson, J. P. Toennies, and C. H. Wöll, Phys. Rev. Lett. **57**, 471 (1986).

[5] B. J. Hinch, A. Lock, J. P. Toennies, and G. Zhang, J. Vac. Sci. Technol. B **7**, 1260 (1989); B. J. Hinch, Phys. Rev. B **38**, 5260 (1988); B. J. Hinch and J. P. Toennies, *ibid.* **42**, 1209 (1990).

[6] For example, M. Henzler, in *Electron Spectroscopy for Surface Analysis*, edited by H. Ibach (Springer, Berlin, 1977).

[7] S. V. Krishnaswamy, G. Derry, D. Wesner, T. J. O'Gorman, and D. R. Frankl, Surf. Sci. **77**, 493 (1978).

[8] G. Boato, P. Cantini, and L. Mattera, Surf. Sci. **55**, 141 (1976).

[9] K. J. McGann and V. Celli, Surf. Sci. **61**, 10 (1976).

[10] E. G. McRae and C. W. Caldwell, Surf. Sci. **7**, 41 (1967); E. G. McRae, *ibid.* **25**, 491 (1971).

[11] N. Cabrera and J. Solana, in *Proceedings of the International*

School of Physics "Enrico Fermi," Varenna, Italy, 1974, edited by F. O. Goodman (Compositori, Bologna, 1974), p. 530.
[12] N. García and W. A. Schlup, Surf. Sci. **122**, L657 (1982).
[13] G. Armand and J. R. Manson, Surf. Sci. **169**, 216 (1986).
[14] S. Miret-Artés, J. Margalef-Roig, R. Guantes, F. Borondo, and C. Jaffé, Phys. Rev. B **54**, 10 397 (1996).
[15] R. Guantes, F. Borondo, C. Jaffé, and S. Miret-Artés, Phys. Rev. B **53**, 14 117 (1996).
[16] D. Farías, M. Patting, K.-H. Rieder, and J. R. Manson, Surf. Sci. **480**, L395 (2001).
[17] A. Glebov, J. R. Manson, J. G. Skofronick, and J. P. Toennies, Phys. Rev. Lett. **78**, 1508 (1997); Phys. Rev. B **58**, 10 012 (1999).
[18] T. Engel and K.-H. Rieder, Surf. Sci. **109**, 140 (1981).
[19] R. Apel, D. Farías, H. Tröger, E. Kirsten, and K. H. Rieder, Surf. Sci. **364**, 303 (1996).
[20] R. Apel, D. Farías, H. Tröger, and K.-H. Rieder, Surf. Sci. **331/333**, 57 (1995).
[21] W. Nichtl-Pecher, W. Stammler, K. Heinz, and K. Müller, Phys. Rev. B **43**, 6946 (1991).
[22] D. Farías and K. H. Rieder, Rep. Prog. Phys. **61**, 1575 (1998).
[23] N. Garcia, V. Celli, and F. O. Goodman, Phys. Rev. B **19**, 634 (1979); V. Celli, N. Garcia, and J. Hutchinson, Surf. Sci. **87**, 112 (1979).
[24] K. L. Wolfe and J. H. Weare, Phys. Rev. Lett. **41**, 1663 (1978); Surf. Sci. **94**, 581 (1980).
[25] J. W. Strutt, (Lord Rayleigh), Proc. R. Soc. London, Ser. A **79**, 399 (1907); *The Theory of Sound* (Dover, New York, 1945), Vol. II.
[26] M. Born and E. Wolf, *Principles of Optics* (Pergamon, London, 1975).
[27] M. Patting, D. Farías, and K.-H. Rieder, Phys. Rev. B **62**, 2108 (2000).
[28] F. Hofmann and J. P. Toennies, Chem. Rev. **96**, 1307 (1996).
[29] E. G. McRae, Rev. Mod. Phys. **51**, 541 (1979).
[30] M. Rocca and F. Moresco, Phys. Rev. Lett. **73**, 822 (1994).